

## **Supplementary Information**

# **High geothermal heat flow beneath Thwaites Glacier in West Antarctica inferred from aeromagnetic data**

**Authors:** Ricarda Dziadek<sup>1,2</sup>, Fausto Ferraccioli<sup>3,4</sup> and Karsten Gohl<sup>1</sup>

## **Supplementary Information Content**

1.	Supplementary Method .....	1
1.1	Overview .....	1
1.2	Magnetic anomaly data processing .....	2
1.3	Curie depth estimates .....	2
2.	Supplementary Discussion .....	3
2.1	Considerations on Curie depth uncertainties .....	3
2.1.1	Satellite data .....	3
2.1.2	Window size .....	3
2.1.3	Long-wavelength contamination .....	4
2.1.4	Wavenumber .....	4
2.1.5	Tectonic setting .....	4
2.2	Considerations on geothermal heat flow uncertainties .....	5
3.	Supplementary References .....	5
4.	Supplementary Table 1 .....	6
5.	Supplementary Figures 1-4 .....	7

### **1. Supplementary Method**

#### **1.1 Overview**

This Supporting Information includes a detailed description of the magnetic anomaly data processing, the spectral method obtaining the Curie depth estimates, followed by considerations on Curie depth uncertainties. Furthermore, the uncertainties of geothermal heat flow determinations are described, based on the standard deviation of the Curie depth estimates. All maps are in polar stereographic projection.

## 1.2 Magnetic anomaly data processing

We expanded the AWI helicopter-borne magnetic grid<sup>1</sup> with 14 flights (~2880 km total survey line length) during RV Polarstern expedition PS104 (2017) in the inner Amundsen Sea Embayment (Supplementary Figure 1a).

The onboard BO-105 helicopter was equipped with a caesium-vapour magnetometer, which was towed with a 30 m long cable. Westward flight directions showed strong noise in the data, which was likely caused by a combination of sensor mounting and orientation of the regional magnetic field. The initial data processing with Geosoft Oasis montajTM included visual editing of obvious erroneous data and low-pass filtering for noise reduction. Measurements during the change in the helicopters flight tracks were removed entirely.

The International Geomagnetic Reference Field (IGRF) of 2015 was removed from the data. In several cross-point iterations we leveled the 2017 flight lines onto the previously reprocessed AWI grid. No base-station correction could be applied, therefore the data may still be affected by diurnal variations in the geomagnetic field. To compensate for the lacking base-station correction the long-wavelength domain (250 - 300 km) was analyzed. The data was then referenced to the Magnetic Field Model MF7 in the region and DC shift of ~ -30 nT was applied to the entire grid.

Applying the same routine to the AGASEA data set onshore resulted in a DC shift of +15 nT, followed by several leveling iterations, where the entire onshore grids were combined and then leveled the AWI grid onto the onshore data sets (AGASEA, BBAS, TORUS). We had planned to increase the number of crossing points in the coastal areas between the different on- and offshore flight campaigns, but did not succeed due to weather conditions, therefore we could use only 4 cross-point calculations, which however did not exhibit a large offset (> 50 nT). Further processing steps involved the extraction of ADMAP2 survey lines (shown in grey in Supplementary Figure 1) adjacent to the working area. These include data from the projects GIMBLE, Casertz, GITARA WMBL, JB + SPRI, USAC + PMagnet + Icegrav, WSE + SAE, BAS IM, Magnet, and USGS. These lines were then gridded and knitted to the previously processed grids. In areas, where no flight lines are available we substituted gaps with the MF7 grid. The main processing steps are summarized in Supplementary Table 1.

## 1.3 Curie depth estimates

We calculated the depth-to-the-bottom of the magnetic source ( $Z_b$ ) with the centroid method<sup>2</sup>, which in first approximation resembles the Curie point depth. The Curie point depth marks a transition zone, rather than an exact depth, where the crustal rocks lose their ferromagnetic magnetization, as a result of increasing temperature with depth above the Curie temperature<sup>3</sup>. Curie depth estimates assume a

homogenous distribution of magnetic minerals, the main magnetic source being magnetite and thus with a Curie temperature of 580°C<sup>4,5,6</sup>. This assumption neglects the compositional variability in plutonic rocks that lead to Curie temperature ranges between 300°C and 680°C, and in cases of magnetic assemblages of Fe-Ni-Co-Cu metal alloys up to 620°C to 1084°C<sup>3</sup>. Without further constraints and validations, these assumptions remain the best guess, especially in sparsely sampled regions like Antarctica, but introduce uncertainties of several kilometers in Curie depths and hence geothermal heat flow (GHF) estimates<sup>5,7</sup>.

After analyzing various magnetic window sizes (100x100 km, 200x200 km and 300x300 km), window sizes of 200x200 km gave optimal results. 100 km were too small to capture the deepest signals, and 300 km tend to average different tectonic regimes. The windows were extracted equidistantly (spacing 50 km) from the newly compiled magnetic anomaly grid presented in this study (Supplementary Figure 1b). Following the method after Tanaka et al. (1999)<sup>2</sup>, the top bound ( $Z_t$ ) and the centroid ( $Z_0$ ) of a magnetic layer composed of a horizontal (equivalent) layer are estimated by fitting a straight line through the intermediate- and low-wavenumber parts of the radially averaged spectrum of  $\ln[(\Phi_{\Delta T}(|k|)^{1/2})]$  and  $\ln\{[\Phi_{\Delta T}(|k|)^{1/2}]/k\}$ , respectively (Supplementary Figure 2). We chose this wavenumber range to estimate  $Z_t$  due to the relatively large flight line spacing. This conservative approach limits the effect of overestimating  $Z_b$  and potentially leading to unrealistically shallow Curie depth estimates.

The basal depth of the magnetic source is thus calculated from the linear relationship between top and centroid depth:  $Z_b = 2Z_0 - Z_t$ . The basal depth of the magnetic source is then assumed to be the Curie point depth and reflects the average value over the window analysed.

## 2. Supplementary Discussion

### 2.1 Considerations on Curie depth uncertainties

#### 2.1.1 Satellite data

Magnetic anomalies derived from satellite data likely permit the usage of this method, as their spatial resolution is not high enough to detect the magnetic source bodies. Hence, in this study we marked the areas where low line coverage or only satellite data is available. Curie depth estimates in these areas should be interpreted with caution or neglected in general. To have full coverage of the area, however, we decided to include the estimates, but do not take the results into account for our discussion and conclusion.

#### 2.1.2 Window size

The dimension of the region must be sufficiently large to capture the deepest magnetic layer and disparate tectonic regimes are not averaged. Ravat et al. (2007)<sup>7</sup> elaborate that the dimension of the

windows analyzed may need to be, in some cases, up to ten times the depth to the bottom, but find that dimensions of more than 200-300 km (Supplementary Figure 3a,b) are less practical. We focus primarily on the results of 200x200 km window sizes. Choosing the window size forces a trade-off between accurately determining  $Z_b$  within each subregion and resolving small changes in  $Z_b$  across subregions<sup>8</sup>. In comparison with larger window sizes of 300x300 km (Supplementary Figure 3b) the overall geometry is preserved. The average of both window sizes (Supplementary Figure 3c) is considered a robust and conservative estimate. The Curie depth map resolution for larger window sizes is subdued and certain features cannot be resolved, for instance, around Thurston Island or Pine Island catchment region. Statistical uncertainties deviate on average by 0.4 km, northeast of Thurston Island and west of Mount Takahe by ~2 km (Supplementary Figure 3d,e). We find that 200x200 km windows resolve certain features well, particularly in the focus regions on Thwaites and Pine Island glaciers.

#### *2.1.3 Long-wavelength contamination*

Further, regional-scale magnetic anomaly databases are usually a mosaic of individual aeromagnetic surveys. Ross et al. (2006)<sup>8</sup> emphasize that subtle discontinuities along survey boundaries are caused by differences in survey specifications, such as flight line spacing, flight altitude, regional field removal, or the quality of data acquisition. The generation of false long-wavelength noise to the regional compilation caused by survey discontinuities or data processing (e.g. DC shift to MF7) may contaminate the long wavelength signal caused by deep magnetic sources, and in turn, affect Curie depth estimates.

#### *2.1.4 Wavenumber*

The centroid depth method allows for a range of possible Curie depth estimates, as the linear regression along the spectral analysis is non-unique. We use a fixed wavenumber range to obtain centroid (0.001-0.005) and top (0.005-0.014) depths, which might increase the uncertainties up to 2 km. Tests with varying ranges for wavenumbers did not change the general distribution of the Curie point depth. We calculated the standard deviation for the Curie estimates (Supplementary Figure 4), which provides some view on the uncertainty distribution, as it is calculated for a fixed range of wavenumbers.

#### *2.1.5 Tectonic setting*

We cannot rule out that younger intrusions into the older basement overprints the magnetic signal and shield the signal of the deepest magnetic layer.

## 2.2 Considerations on geothermal heat flow uncertainties

We approximated the geothermal heat flow based on the Curie depth uncertainties in a steady-state model of a homogenous material via

$$Q = -k \frac{\partial T}{\partial z} \quad (1)$$

Where  $Q$  is the heat flow at the bed surface (in mW/m<sup>2</sup>),  $T$  is the Curie temperature (580°C),  $z$  the Curie depth (in km), and  $k$  the thermal conductivity of the lithosphere (2.2 W/mK)<sup>9,10</sup>. The uncertainties are shown in Supplementary Figure 4.

Although a range of parameters contribute to geothermal heat flow in general, such as varying crustal composition or radiogenic heat production, we did not account for these parameters, because they are poorly constraint in the working area. We note, that while geophysical methods remain the best approach to estimate GHF in Antarctica<sup>11</sup>, results vary in magnitude and distribution. The largest uncertainty in all geophysical models stems from the uncertainty in composition and structure of the lithosphere and mantle. The linear translation of GHF from Curie depth estimates thus provides a base for discussing the shape of thermal anomalies. The limitations of the method should be considered, when analyzing absolute GHF values, which in this case represent the lower range of the GHF spectrum.

## 3. Supplementary References

1. Gohl, K., Denk, A., Eagles, G. & Wobbe, F. Deciphering tectonic phases of the Amundsen Sea Embayment shelf, West Antarctica, from a magnetic anomaly grid. *Tectonophysics* 585, 113–123, doi:10.1016/j.tecto.2012.06.036 (2013).
2. Tanaka, A., Okubo, Y. & Matsubayashi, O. Curie point depth based on spectrum analysis of the magnetic anomaly data in East and Southeast Asia. *Tectonophysics* 306, 461–470, doi:10.1016/S0040-1951(99)00072-4 (1999).
3. Haggerty, S. E. Mineralogical constraints on curie isotherms in deep crustal magnetic anomalies. *Geophys. Res. Lett.* 5, 105–108, doi:10.1029/GL005i002p00105 (1978).
4. Fox Maule, C., Purucker, M. E., Olsen, N. & Mosegaard, K. Heat flux anomalies in Antarctica revealed by satellite magnetic data. *Science* 309, 464–467, doi:10.1126/science.1106888 (2005).
5. Bansal, A. R., Gabriel, G., Dimri, V. P. & Krawczyk, C.M. Estimation of depth to the bottom of magnetic sources by a modified centroid method for fractal distribution of sources: An application to aeromagnetic data in Germany. *Geophysics* 76, L11–L22, doi:10.1190/1.3560017 (2011).
6. Langel, R. A. & Hinze, W. J. *The Magnetic Field of the Earth's Lithosphere*. Cambridge University Press, Cambridge, ISBN 0521473330 (1998).
7. Ravat, D., Pignatelli, A., Nicolosi, I. & Chiappini, M. A study of spectral methods of estimating

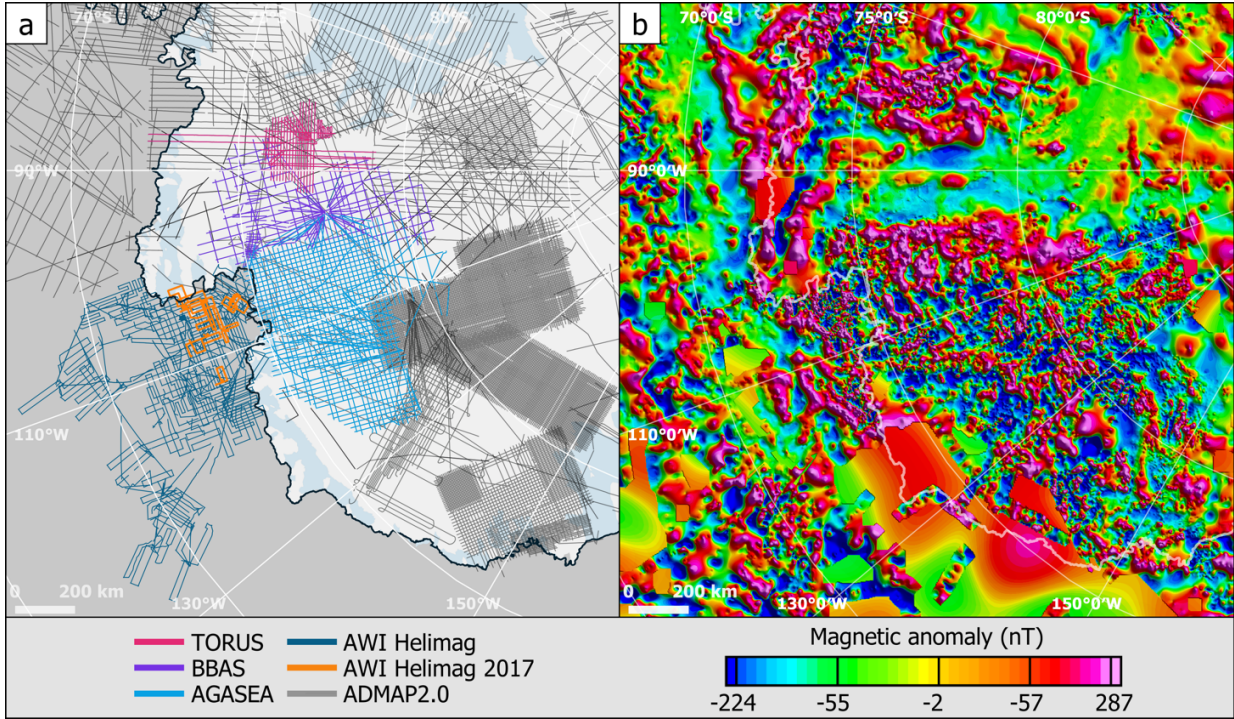
- the depth to the bottom of magnetic sources from near-surface magnetic anomaly data. *Geophys. J. Int.* 169, 421–434, doi:10.1111/j.1365-246X.2007.03305.x (2007).
8. Ross, H. E., Blakely, R. J. & Zoback, M. D. Testing the use of aeromagnetic data for the determination of Curie depth in California. *Geophysics* 71, L51–L59, doi:10.1190/1.2335572 (2006).
  9. Hasterok, D. & Chapman, D. S. Heat production and geotherms for the continental lithosphere. *Earth Planet. Sci. Lett.* 307, 59–70, doi:10.1016/j.epsl.2011.04.034 (2011).
  10. Kappelmeyer, O. & Haenel, R. *Geothermics with special reference to applications*, Vol. 4, Gebrüder Borntraeger, Berlin (1974).
  11. Burton-Johnson, A., Dziadek, R. & Martin, C. Review article: Geothermal heat flow in Antarctica: current and future directions. *Cryosph.* 14, 3843–3873, doi:10.5194/tc-14-3843-2020 (2020).

#### 4. Supplementary Table 1

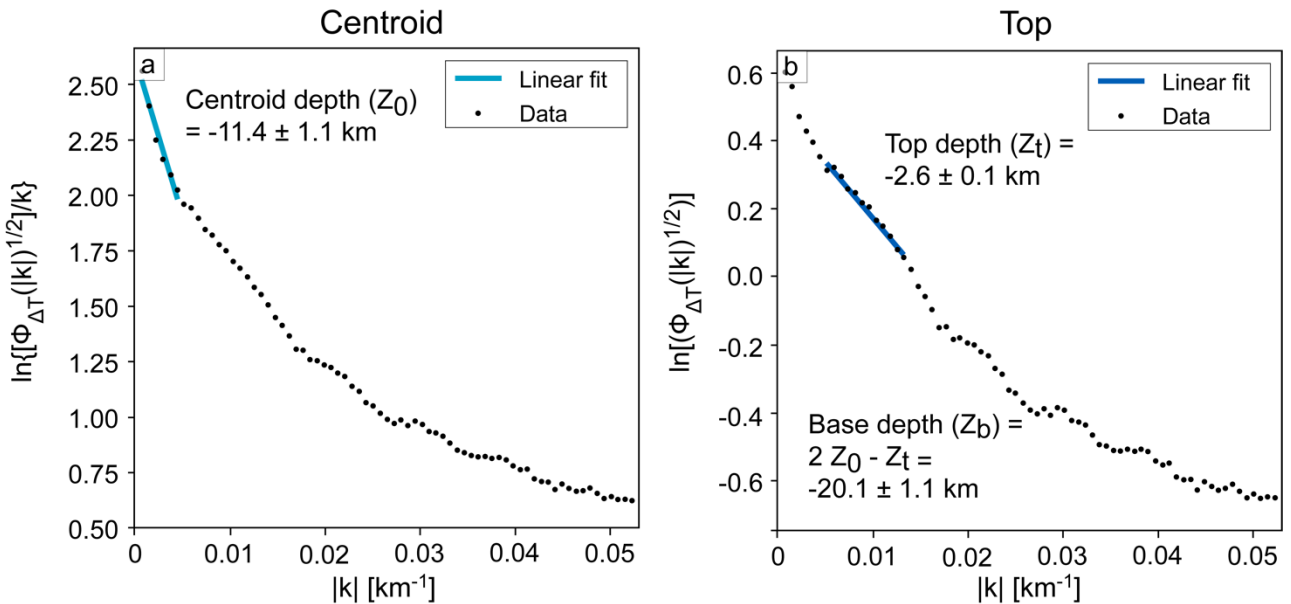
**Supplementary Table 1.** Processing steps for magnetic anomaly data.

Dataset	Processing steps
(1) AWI	Include 2017 flight lines, de-spiking, line-splitting, IGRF2015 removal, filtering, cross-point analysis, tension spline corrections, several leveling iterations, DC shift to MF7, gridding
(2) BBAS	Include unpublished flight lines, cross-point analysis, several leveling iterations, DC shift to MF7, gridding
(3) TORUS	Include unpublished flight lines, cross-point analysis, several leveling iterations, DC shift to MF7, gridding
(4) AGASEA	Include unpublished flight lines, cross-point analysis, several leveling iterations, DC shift to MF7, gridding
(5) ADMAP2.0	Extraction of surveys from database adjacent to working area
(1) – (4)	Cross-point analysis, several leveling iterations, gridding
(1) – (5)	Grid knitting
(2) New grid	Substitute NaNs/data gaps with MF7

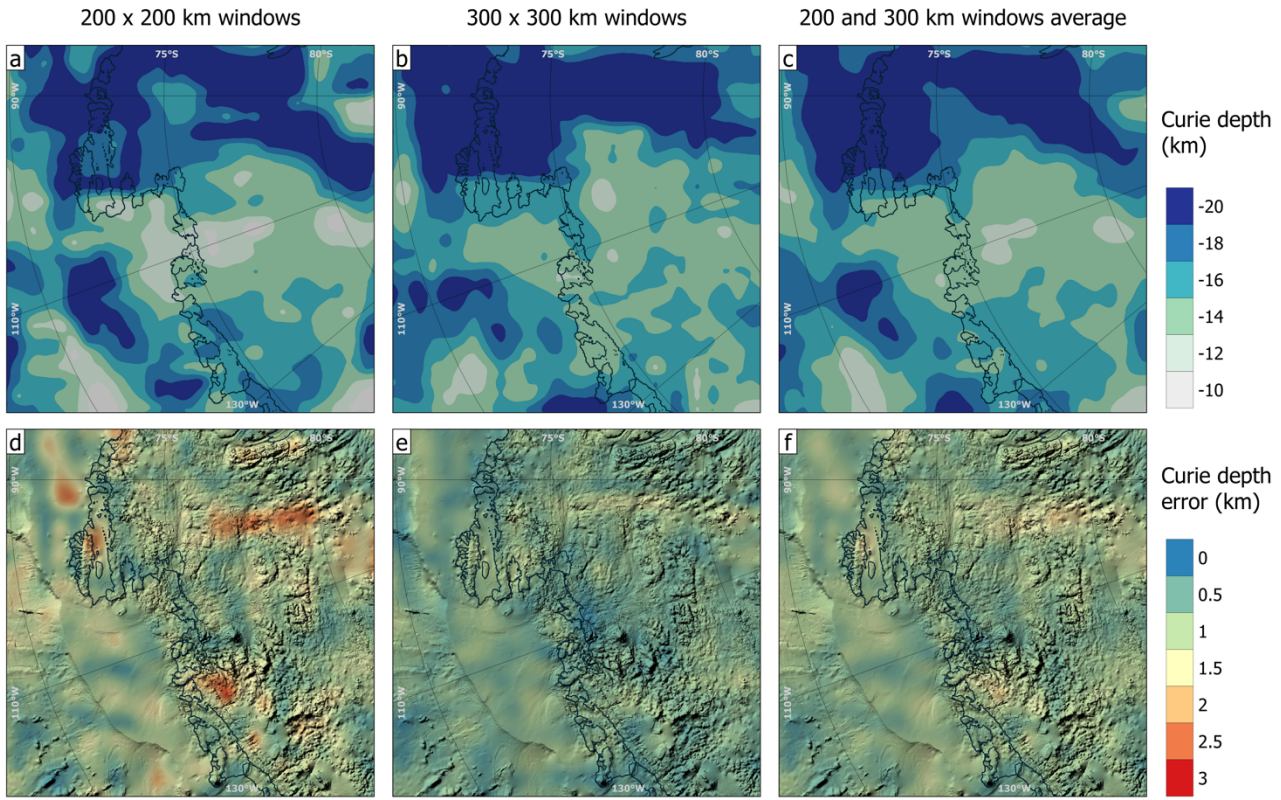
## 5. Supplementary Figures 1-4



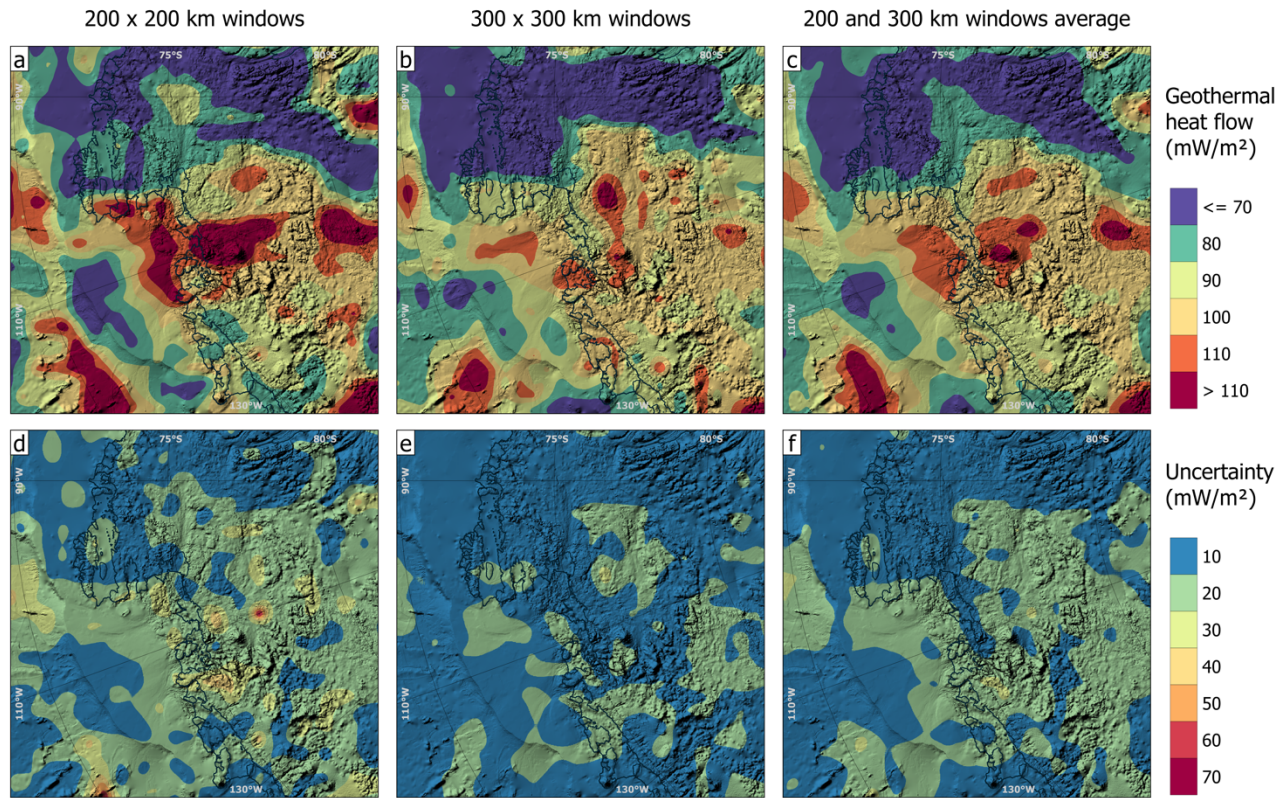
**Supplementary Figure 1. Overview on flight line coverage and magnetic anomalies.** **a)** Flight line coverage in the region. Reprocessed lines are color-coded. **b)** Gridded magnetic anomaly dataset for the region.



**Supplementary Figure 2. Example for power spectral analysis of magnetic anomaly data.** **a)** The centroid depth ( $Z_0$ ) is obtained from the in the lower wavenumber range of the spectrum. **b)** The top depth ( $Z_t$ ) is obtained from the low to intermediate wavenumber range of the spectrum and the base depth ( $Z_b$ ) calculated from the linear relationship between these  $Z_0$  and  $Z_t$ .



**Supplementary Figure 3.** Results of Curie depth analysis with varying window sizes and their respective uncertainties. **a)** Curie depth model based on a 200x200 km window size as discussed primarily in this study. **b)** Curie depth model based on 300x300 km window size. **c)** Curie depth model based on average of (a) and (b). **d-f)** Standard deviation of Curie depth estimates for a fixed wavenumber range. Largest error are  $\pm 2.7$  km and occur south of Ellsworth-Whitmore mountains and towards Marie Byrd Land.



**Supplementary Figure 4. Geothermal heat flow and uncertainties.** *a-c)* Geothermal heat flow estimates based on Curie depth estimates with varying window sizes and their average. *d-f)* Uncertainty of geothermal heat flow based on Curie depth standard deviation for varying window sizes and their average.